hydrology

MDPI

Article

# Catchment Hydrology during Winter and Spring and the Link to Soil Erosion: A Case Study in Norway

**Torsten Starkloff [1,*], Rudi Hessel [2], Jannes Stolte [1] and Coen Ritsema [2]**

1 Norwegian Institute of Bioeconomy Research (NIBIO), Fredrik A Dahlsvei 20, N-1431 Ås, Norway; Jannes.Stolte@nibio.no

2 Wageningen Environmental Research (Alterra), P.O. Box 47, 6700 AA Wageningen, The Netherlands; rudi.hessel@wur.nl (R.H.); Coen.Ritsema@wur.nl (C.R.)

* Correspondence: torsten.starkloff@nibio.no; Tel.: +47-469-32-253

Academic Editor: Okke Batelaan

Received: 2 January 2017; Accepted: 17 February 2017; Published: 23 February 2017

**Abstract:** In the Nordic countries, soil erosion rates in winter and early spring can exceed those at other times of the year. In particular, snowmelt, combined with rain and soil frost, leads to severe soil erosion, even, e.g., in low risk areas in Norway. In southern Norway, previous attempts to predict soil erosion during winter and spring have not been very accurate owing to a lack of catchment-based data, resulting in a poor understanding of hydrological processes during winter. Therefore, a field study was carried out over three consecutive winters (2013, 2014 and 2015) to gather relevant data. In parallel, the development of the snow cover, soil temperature and ice content during these three winters was simulated with the Simultaneous Heat and Water (SHAW) model for two different soils (sand, clay). The field observations carried out in winter revealed high complexity and diversity in the hydrological processes occurring in the catchment. Major soil erosion was caused by a small rain event on frozen ground before snow cover was established, while snowmelt played no significant role in terms of soil erosion in the study period. Four factors that determine the extent of runoff and erosion were of particular importance: (1) soil water content at freezing; (2) whether soil is frozen or unfrozen at a particular moment; (3) the state of the snow pack; and (4) tillage practices prior to winter. SHAW performed well in this application and proved that it is a valuable tool for investigating and simulating snow cover development, soil temperature and extent of freezing in soil profiles.

**Keywords:** SHAW; soil freezing; snow; infiltration; modelling; soil erosion

## 1. Introduction

In the Nordic countries, soil erosion rates in winter and early spring can exceed those occurring during other seasons of the year. A factor of particular importance is the incidence of frozen soil, which modifies surface runoff generation and also the erosivity of the soil material [1]. In addition, water infiltration into frozen soils is more complicated than water infiltration into unfrozen soils, because it involves coupling water and heat transport (temperature of the infiltrating water) with phase change (from liquid to ice and vice versa) [2].

A large number of laboratory studies has investigated different processes occurring in soils during freezing and thawing. Using a rain simulator, Edwards and Burney [3] showed that soil freezing and thawing can significantly increase soil erosivity. They concluded that only plant cover is effective in reducing soil losses due to rain and overland flow on frozen ground. Other more recent studies, e.g., Ban et al. [4], have shown that water flows much faster over a frozen slope than over a thawed slope. Watanabe et al. [5] found that the speed of snowmelt and/or rain infiltration into frozen soils is largely dependent on initial water content, frost depth and temperature of the soil. In addition,

Yami et al. [6] showed that increasing soil moisture and finer soil structure advance the speed and depth of the freezing front.

Al-Houri et al. [7] added to knowledge about water transport in frozen soils by showing that the amount of time available for soil water redistribution before freezing affects the infiltration capacity of frozen soil, with more time resulting in better infiltration capacity under frozen conditions. In addition to laboratory studies, a great number of studies has investigated infiltration processes under field conditions at the plot or point scale. In a study examining nine different plots in North Dakota, Willis et al. [8] showed that soils that were dry in autumn freeze faster and deeper than wet soils and that a dry profile thaws upward, while a wet soil thaws both upward and downward. They also recorded less runoff from dry soils.

Stähli et al. [9] and Nyberg et al. [10] concluded that frost has little effect on runoff from forest soils, in contrast to reported effects on agricultural soils [11], and that forests probably do not increase runoff episodes in winter and spring. Furthermore, they predicted that critical initial conditions, such as high water content and early frost penetration combined with heavy rain on still frozen soil, could have a decisive effect on the amount of runoff. Iwata et al. [12,13] showed that a frozen soil layer can significantly impede snowmelt infiltration and thus increase runoff of spring snowmelt water. Zhao et al. [13] demonstrated that soil freezing can reduce hydraulic conductivity by blocking pores and retaining water in the profile, thereby reducing the infiltration capacity during snowmelt.

In a study at five locations in Finland, Sutinen et al. [14] found that a snow pack with a thickness exceeding 30 cm can reduce or even prevent soil freezing. In addition, Zhao et al. [15] showed that snow pack less than 20 cm deep can cause deeper soil freezing than no snow cover, due to an increase in ground albedo caused by the snow. The effects of different tillage practices on soil freezing was investigated by Parkin et al. [16] in a soil profile over 10 years. They found that conventional autumn tillage resulted in lower soil temperatures than no-till.

In a recent five-year field study in Canada, He et al. [17] presented results that confirmed many of the above-mentioned effects and demonstrated the complexity of the interaction between the topsoil and snow cover, especially during snowmelt. They also pointed out that only a limited amount of field studies to date has taken all of these processes into account in a series of measurements that covers several winter periods. The complexity of the different processes occurring in soil during winter is amplified when all of these interacting processes have to be monitored and interpreted at the catchment scale, where different soil types, terrain and water flow at the surface and in the soils interact [18,19]. In addition, detailed observations have to be made over several years to identify processes that can only occur during certain conditions or are masked by confounding factors in a catchment [20].

In Norway, the incidence of soil erosion from agricultural land is greatest during spring [21,22], and the severity of the erosion is often amplified by preceding winter conditions. Snowmelt, combined with rain and soil frost, can lead to severe gully and rill erosion, even in low risk areas in Norway [23]. In southern Norway, previous attempts to predict soil erosion during winter and spring have not been very accurate [24], probably owing to a lack of catchment-based studies covering several winters, resulting in a lack of knowledge about the interacting processes described above. In the present study, field measurements covering three winter periods (2013, 2014 and 2015) were carried out, with the aim of improving overall understanding of how soil hydraulic properties behave during winter and affect surface runoff caused by snowmelt and rain and how these processes are linked to soil erosion. Furthermore, the data collected were used to calibrate and validate a hydrodynamic model (Simultaneous Heat and Water (SHAW) model; [25], in order to acquire better insights into the complex interactions between freezing, thawing, snowpack and runoff and erosion dynamics.

The focus of this study lies in Norway; however, severe soil erosion on agricultural areas during winter and spring is a problem in many other countries around the world (e.g., USA [26], Belgium [27], the U.K. [28], Germany [29], Russia [30]). In these areas, like in Norway, soil erosion during winter and spring depletes the irreplaceable nutrient-rich top layer of agricultural soils and results in a major part of the annual input of phosphorous and nitrogen from agricultural catchments to fresh water

bodies [31]. It is therefore hoped that this study will also contribute to the understanding of winter processes outside of Norway.

## 2. Methodology

### *2.1. Study Area*

The study area is located in the Skuterud catchment (4.5 km$^2$) in Ås and Ski municipalities, approximately 30 km south of Oslo, Norway. For the field investigations and sampling, a sub-catchment, Gryteland (0.29 km$^2$), in the southeastern part of the main catchment (Figure 1), was chosen. This area has been used for different hydrological studies in the past, and it can easily be reached under all weather conditions. A monitoring station was installed at the outlet of the sub-catchment in 2008. This station measures precipitation, air temperature, surface runoff and drainage discharge. In addition, five stations (one at the outlet) were installed along a transect in the catchment [32] (Figure 1), in order to measure soil moisture and soil temperature at three depths (5, 10 and 20 cm).

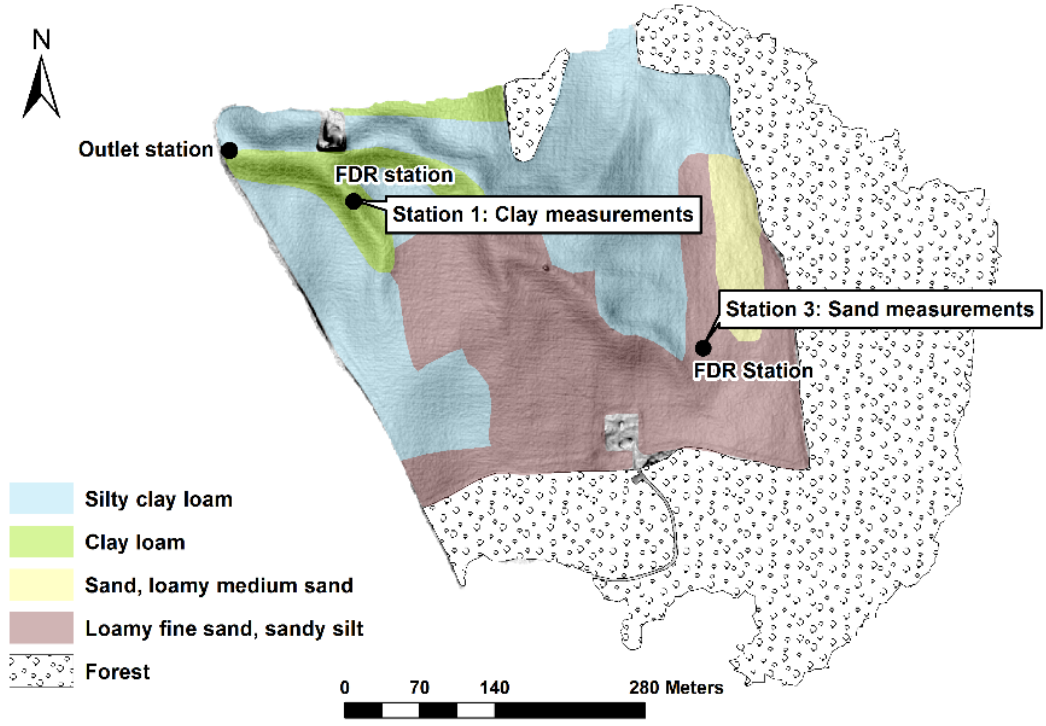


**Figure 1.** Soil and hill shade map of the Gryteland catchment in southern Norway. FDR, Frequency Domain Reflectometry.

The sub-catchment is characterized by an undulating landscape (elevation 106–141 m, slope 2%–10%) covered by approximately 60% arable land and 40% coniferous forest. Soil types for the arable land are a levelled clay loam (Stagnosol) and a silty clay loam (Albeluvisol) (Group 1), as well as a sandy silt on clay (Umbrisol) and a sand to loamy medium sand (Histic Gleysol) (Group 2). The two soil groups are often not clearly distinguishable in the field. Within the groups, the soils have similar physical properties. Hereafter, Groups 1 and 2 are referred to as clay and sand, respectively (Figure 1).

Mean annual temperature in the study area is 5.3 °C, with an average minimum of −4.8 °C in January/February and an average maximum of 16.1 °C in July. Mean annual precipitation is 785 mm, with a minimum monthly amount of 35 mm in February and a maximum of 100 mm in October [33]. Winter is usually relatively unstable, with alternating periods of freezing and thawing and several snowmelt events [34].

There was no tillage (no-till system) after harvest in 2013, leaving the fields covered in stubble. In 2014 and 2015, secondary tillage was performed after harvest with a cultivator on the slopes, leaving the depressions still covered with stubble.

### *2.2. Weather Data*

A weather station was installed in the catchment outlet at the end of 2013, providing hourly data on net solar radiation, air temperature, wind speed and wind direction for the winters (December–March) of 2014 and 2015. For winter 2013 (January–April), data from a station 6 km away from the catchment were used ([33].

### *2.3. Soil Temperature and Soil Moisture Measurements*

To obtain more detailed measurements of soil water content and temperature during winter, the measuring Stations 1 (clay measurements) and 3 (sand measurements) were upgraded to measure soil water content and soil temperature at four depths, 5, 20, 30 and 40 cm, using Decagon 5 TM temperature and Frequency Domain Reflectometry (FDR) sensors. Measurements from these two stations and the outlet station were used in the present study. However, it should be noted that the soil water content, calculated from the dielectricity of the soil, measured with the FDR probes, represents only the liquid soil water content, not water in the form of ice, and therefore, only the liquid soil water content

### *2.4. Discharge Measurements*

To estimate how the catchment reacted to precipitation and to analyze the infiltration capacity of the soils in the catchment, data on discharge measured at the outlet were analyzed. Besides measuring how much discharge was produced during the winter periods, the runoff coefficient was calculated as:

$$D_{ro} = 100 \times D_M / P_A$$

where $D_{ro}$ = runoff coefficient (%); $D_M$ = discharge ($m^3$); $P_A$ = precipitation on area ($m^3$).

### *2.5. Snow Cover Properties*

Snow has a significant influence on changes in soil temperature and soil water content [14]. Therefore, snow properties (depth and density) were monitored in the catchment during the three winters. The measurements taken at the outlet, Stations 1 and 3, are presented in this study. Snow Water Equivalent (SWE) was sampled after weather changes expected to result in changes in SWE [35]. The measured snow depth data were used to validate snow depth values simulated with the SHAW model.

### *2.6. Erosion Mapping*

In addition to the other measurements carried out in the field, soil erosion features were documented. Minor erosion damage was recorded by taking pictures. The extent of any large features observed was mapped using a differential GPS, and the depth and width were measured at several points using a ruler.

### *2.7. SHAW Model Setup and Calibration*

The SHAW model, which was originally developed to simulate soil freezing and thawing [36], simulates heat, water and solute transfer within a one-dimensional profile extending downwards from the vegetation canopy to a specified depth within the soil. A layered system is established through the plant canopy, snow, residue and soil, and each layer is represented by an individual node [25]. Infiltration is calculated using a Green–Ampt approach for a multi-layered soil. Water flow in frozen soil is assumed to be similar to flow in unsaturated soil. Therefore, the relationships for matric potential and hydraulic conductivity of unsaturated soils are assumed to be valid for frozen soils. However,

hydraulic conductivity is reduced linearly with ice content, assuming zero conductivity at an available porosity of 0.13 [37]. A detailed description of the model can be found in Flerchinger [38].

Input to the SHAW model includes: initial conditions for snow, soil temperature and water content profiles; daily or hourly weather conditions (temperature, wind speed, humidity, precipitation and solar radiation); general site information; and parameters describing the vegetative cover, snow, plant residues and soil. General site information includes slope, aspect, latitude and surface roughness parameters. Input soil parameters are bulk density, saturated conductivity, albedo and coefficient for the soil water potential-water content relationship [38].

To obtain the necessary soil input data (Table 1), undisturbed samples were taken in April 2014 at three different depths (0, 25 and 35 cm) at Stations 1 and 3. These depths corresponded to the depth between FDR probes, avoiding the disturbed area around the probes. For determination of saturated soil hydraulic conductivity ($K_{sat}$) and saturated water content ($\theta_S$), two samples (volume of sample ring 250 cm$^3$) were taken. Two additional samples (volume of sample ring 98 cm$^3$) were used for determination of bulk density and soil organic matter. In total, 12 samples were taken at each of the two stations.

Saturated soil hydraulic conductivity was determined using the constant head method [39]. The two soil profiles defined for SHAW are presented in Table 1, with the corresponding depths of the simulation nodes (same as the installation depth of the FDR/temperature probes). For the simulations of winter 2013, only the clay was included, as a three-layered soil profile with the location of the nodes at 5, 10 and 20 cm, due to missing data for the sand and only three FDR/temperature probes in the clay.

**Table 1.** Input parameters for the SHAW model. Only the three layers marked with an asterisk (*) were used for the 2013 simulation, and the depth was reduced from 15 down to 10 cm and from 25 cm down to 20 cm.

| **Soil Type** | **Clay** | | | | **Sand** | | | |
|---|---|---|---|---|---|---|---|---|
| Location | 59°40′ N, North Facing (22.5°), Slope 12°, Elevation ASL 100 m | | | | 59°40′ N, Northwest Facing (330.5°), Slope 0°, Elevation ASL 140 m | | | |
| Surface | Albedo of dry soil: 0.15 Wind profile surface roughness: 0.1 cm | | | | | | | |
| Depth | 5 cm * | 15 cm * | 25 cm * | 35 cm | 5 cm | 15 cm | 25 cm | 35 cm |
| Campbell's b | 20 | 20 | 20 | 20 | 3 | 1 | 1 | 1 |
| Air entry potential (hPa) | −31 | −31 | −34 | −35 | −31 | −31 | −34 | −35 |
| $K_{sat}$ (cm·h$^{-1}$) | 2.60 | 1.86 | 1.00 | 0.60 | 16.80 | 18.00 | 22.00 | 24.00 |
| Bulk density (kg·m$^{-3}$) | 1331 | 1400 | 1535 | 1537 | 1190 | 1346 | 1346 | 1347 |
| $\theta_S$ | 0.40 | 0.40 | 0.40 | 0.35 | 0.43 | 0.40 | 0.40 | 0.31 |
| Sand (%) | 13 | | | | 70 | | | |
| Silt (%) | 58 | | | | 13 | | | |
| Clay (%) | 29 | | | | 7 | | | |
| Organic matter content (%) | 4.5 | 4.0 | 3.7 | 3.5 | 3.4 | 3.4 | 2.7 | 2.0 |

The model was calibrated to fit the measured snow depth and soil temperature by adjusting the site-specific parameters maximum temperature at which precipitation is snow ($T_{\max}$) (only for winter 2015) and the wind profile roughness for momentum transfer of the snow cover ($z_m$) (for all three winters).

## 3. Results

### 3.1. Weather Measurements

Measured air temperature and precipitation are presented in Figure 2. Periods with continuous snow cover, indicated with blue bands in the diagram, were of differing duration in the different years.

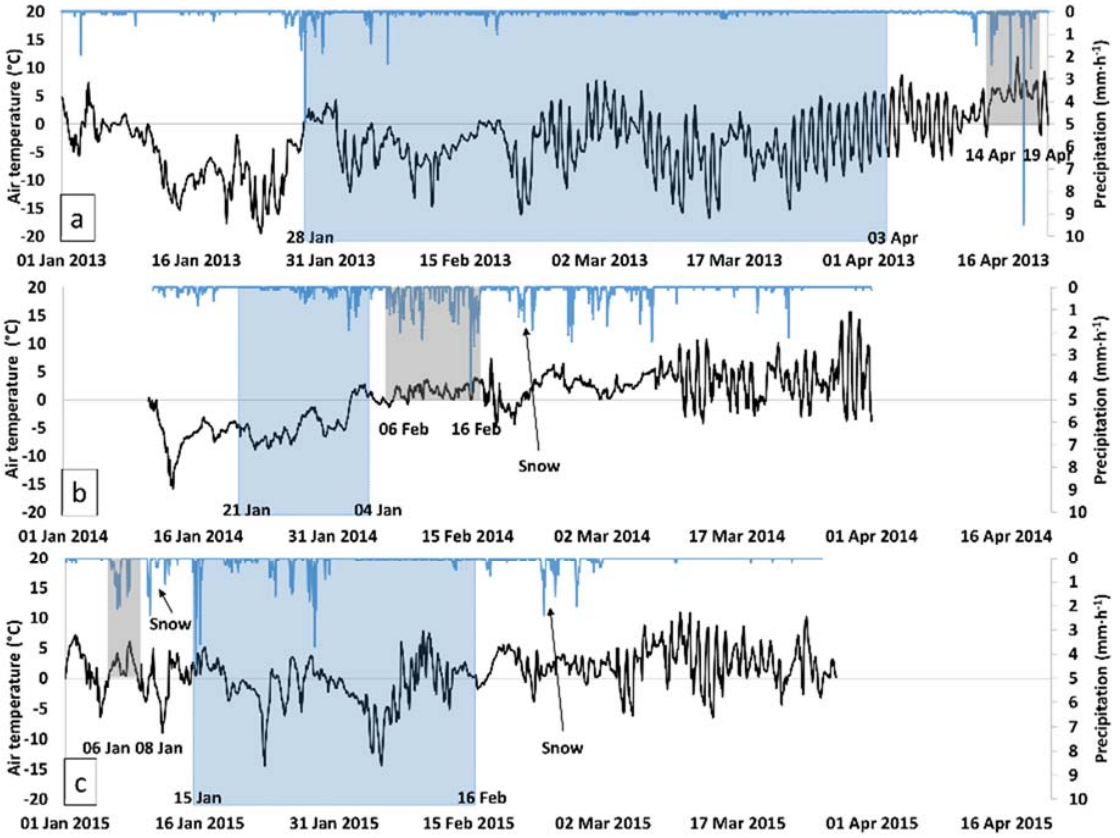


**Figure 2.** Measured air temperature and precipitation for the three winter periods: 2013 (**a**); 2014 (**b**); and 2015 (**c**). Rain events of interest for this study with start and end dates are marked with grey bands. The duration of unbroken snow cover with start and end dates is indicated with blue bands. Snow events outside the unbroken snow cover period are marked as 'snow'.

The number, duration and intensity of rain events during the three winter periods also differed considerably. For each winter period, rain events of interest were selected (grey bands in Figure 2) for detailed analysis. A rain event was classified as 'interesting' for this study when the precipitation fell as rain on completely or partially frozen ground. The total amount of rain and the duration of the 'main event' when the highest measured intensities occurred are shown in Table 2.

**Table 2.** Start and end dates of the rain events of interest, with measured total amount of precipitation, highest measured intensity and the duration and amount of precipitation of the main event within the whole event.

| Date | Total (mm) | Main Event | Highest Intensity (mm·h$^{-1}$) |
|---|---|---|---|
| 14–19 April 2013 | 42.1 | 15.8 mm in 2 h | 9.3 |
| 6–16 February 2014 | 105 | 10 mm in 4 h | 4.6 |
| 6–8 January 2015 | 28 | 7 mm in 4 h | 2.0 |

In terms of intensity, the 2013 event listed in Table 2 would be classified as heavy rain and the other events as moderate rain. The rain event in 2014 occurred on top of ongoing snowmelt after 4 February.

### 3.2. Surface Discharge Measurements

Measured surface discharge for the selected rain events is presented in Table 3, together with the estimated discharge coefficients. The main discharge events in the three winter periods occurred

during these rain events, rather than as a result of snowmelt. While the rain event in 2013 was the largest of the three events, the rain event in 2015 produced the highest amount of discharge and had the highest discharge coefficient. During winter 2014, little discharge was produced by the rain event of interest (1008 $m^3$) compared with the other two years (2594–3096 $m^3$) (Table 3). However, it should be noted that some tunneling below the flume was observed, resulting in the by-pass of water and too low discharge values. This was repaired and did not happen in 2015.

**Table 3.** Start and end date of the rain events of interest with measured surface discharge, precipitation per area and percentage of precipitation water, which reached the outlet (discharge coefficient) for these rain events. Values in parenthesis show the discharge coefficient for the agricultural area only (no forest). Values marked with an asterisk (*) are incorrect measurements due to the by-pass of water below the flume.

| Date | Discharge ($m^3$) | Precipitation ($m^3$) | Discharge Coefficient (%) |
|---|---|---|---|
| 14–19 April 2013 | 3096 | 12,180 | 25 (50) |
| 6–16 February 2014 | 1008 * | 30,450 | 4 * |
| 6–8 January 2015 | 2594 | 8120 | 32 (63) |

By comparing the discharge measured at the Gryteland sub-catchment outlet with discharge measured at the outlet of the main Skuterud catchment, it was determined that a surface discharge coefficient of about 12%, rather than 4%, was more realistic for the event in 2014.

### *3.3. Liquid Soil Water Content and Soil Temperature*

A malfunction in Stations 1 and 3 created a gap in the data for winter 2013. The two stations were repaired just before the extreme event at the end of the winter period, so that soil moisture and soil temperature measurements for the clay and sand were available for this event (insert diagram in Figure 3). For the clay, measured data were taken close by the outlet station, where undisturbed soil moisture and soil temperature data were obtained throughout winter 2013 (Figure 3).

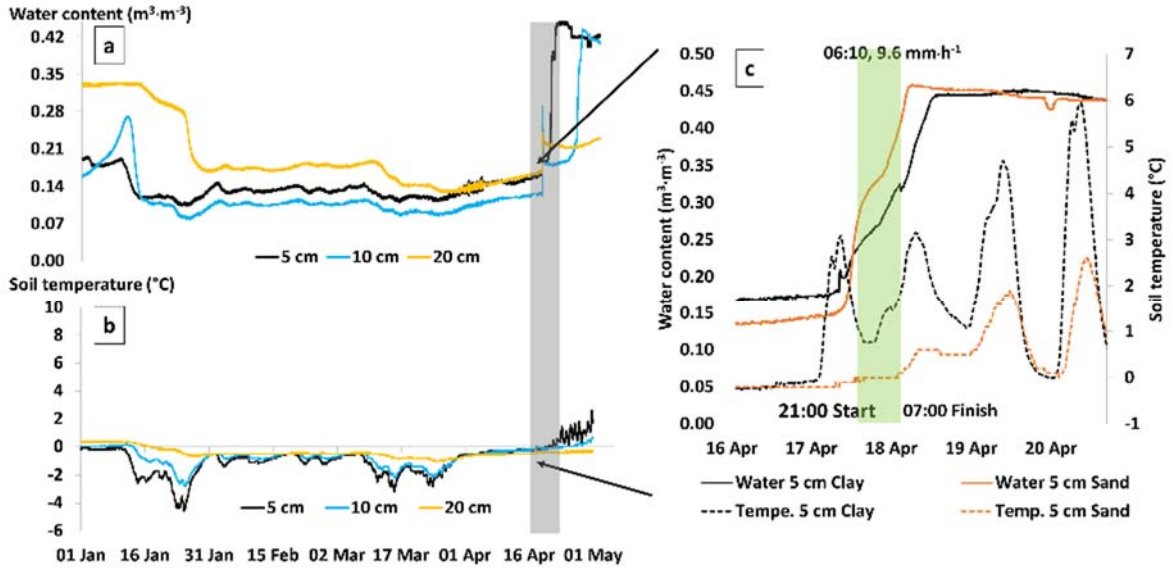


**Figure 3.** Measured soil water content (**a**) and soil temperature (**b**) in the clay during winter 2013 with the insert diagram (**c**) showing measured soil water content and soil temperature at 5 cm depth in the clay and sand during the rain event of interest in 2013 (duration marked with grey band in (**a**,**b**)). The period with the highest precipitation intensities is marked with a green band in (**c**).

During winter 2013, the soil temperature and liquid soil water content measurements were characterized by a long period of soil frost at all soil depths (Figure 3). Shortly after 2 December, the soil started to freeze at 5 and 10 cm and stayed frozen until the highest precipitation intensities (9.6 mm·h$^{-1}$) occurred on 18 March (Figure 3). Frozen soil was indicated by a low liquid soil water content (~0.12 m$^3$·m$^{-3}$) compared with pre-freezing (~0.38 m$^3$·m$^{-3}$ in November 2012) and soil temperature below 0 °C. As can be seen in Figure 3, the soil was still frozen after the first rain event on 14 April. The liquid soil water content was still low in both soils (~0.17 m$^3$·m$^{-3}$ in the clay and 0.13 m$^3$·m$^{-3}$ in the sand), and the measured soil temperature was below 0 °C in both soils. On 17 April, the soil temperature in the top 5 cm in the clay soil started to rise above 0 °C, followed by a continuous increase in liquid soil water content at 5 and 10 cm depth. The soil temperature in the topsoil dropped to about 0.8 °C when the major rain event started in the evening of 17 April. However, the liquid soil water content continued to increase steadily and more rapidly in the sand than in the clay. When the highest precipitation rates occurred, the clay soil had reached a liquid soil water content of about 0.25 m$^3$·m$^{-3}$. The temperature in the sand soil rose much more slowly than in the clay soil, but the liquid soil water content increased rapidly in the sand topsoil layer at the same rate as in the clay soil, reaching a liquid soil water content of 0.34 m$^3$·m$^{-3}$ when the highest precipitation intensities occurred. During the final period of the high intensity rain, the soil water content continued to rise to about 0.45 m$^3$·m$^{-3}$ in both the clay and the sand. No further increase in soil water content occurred during the rest of the rain event, probably because both soils were fully saturated.

Measured soil water content during winter 2014 for the clay and sand is shown in Figure 4, and measured soil temperature is presented in Figure 5.

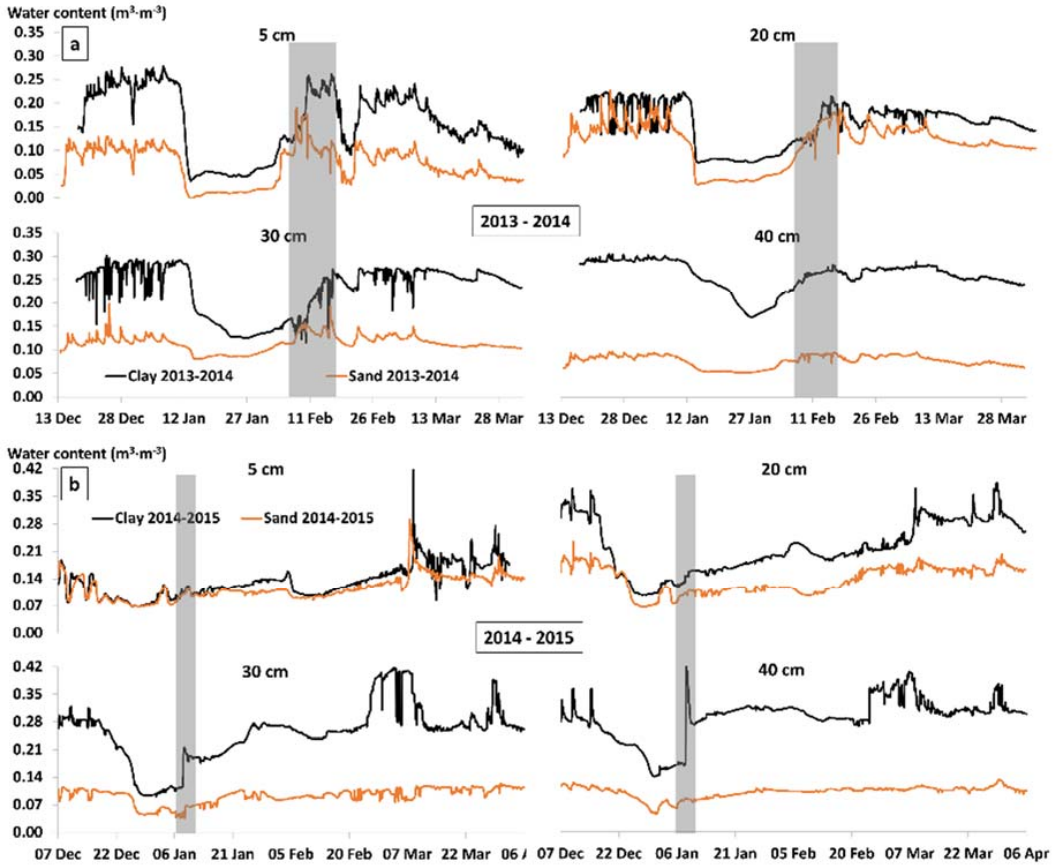


**Figure 4.** Measured soil water content in the clay and sand for the winter periods 2014 (**a**) and 2015 (**b**) at four depths: 5, 20, 30 and 40 cm. Durations of the rain events of interest (according to Table 2) are marked with grey bands.

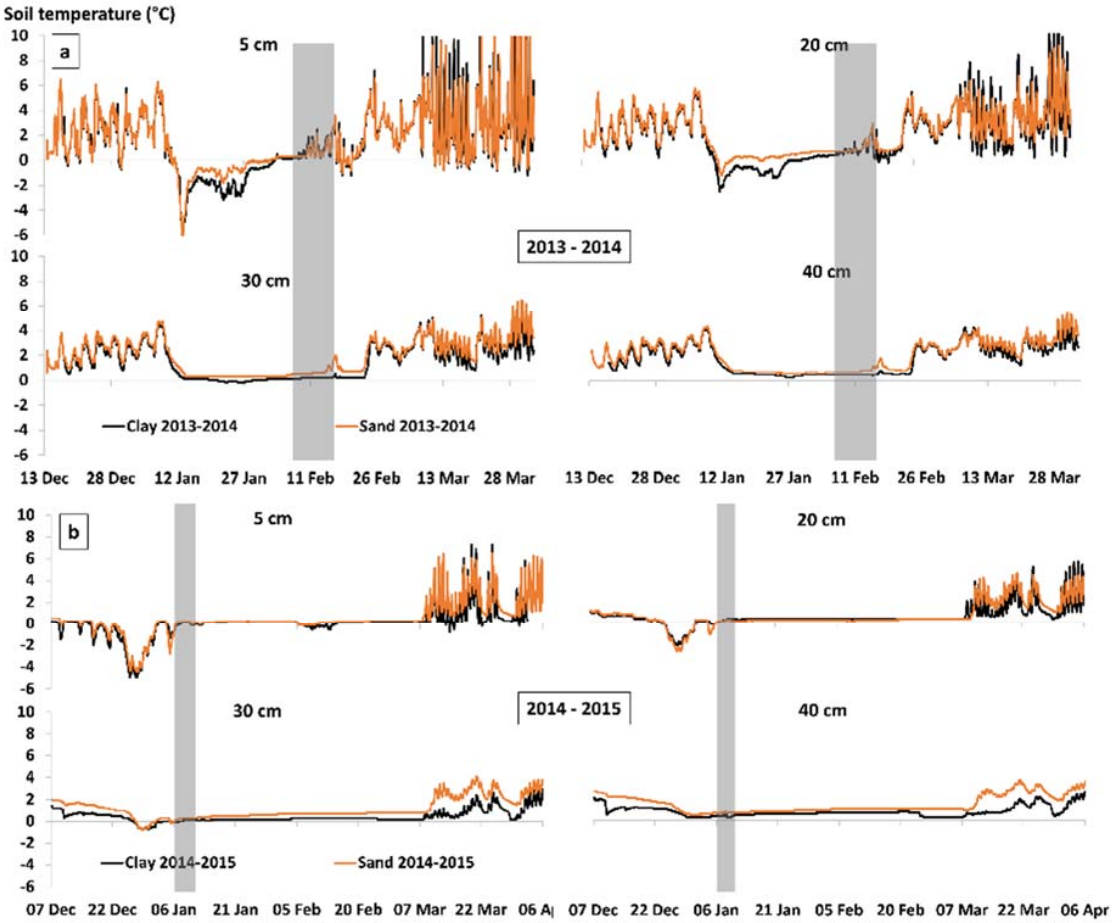


**Figure 5.** Measured soil temperature in the clay and sand for the winter periods 2014 (**a**) and 2015 (**b**) at four depths: 5, 20, 30 and 40 cm. Durations of the rain events of interest (according to Table 2) are marked with grey bands.

Measured soil water content and temperature declined significantly in both the clay and sand immediately after the air temperature started to drop below zero (Figures 4 and 5) around 6 January. Measured soil water content did not change much after 13 January, whereas soil temperature followed the changes in air temperature, although this effect decreased with increasing depth for both soil types. After 27 January, the liquid soil water content rose slowly, due to an increase in air temperature (Figure 2), resulting in thawing of ice in the soil. After 3 February, the liquid soil water content increased rapidly due to incoming snowmelt water. While the soil water content did not change much in the sand at 30 and 40 cm depth, a decrease in liquid soil water content was observed at these depths in the clay. Both soils showed similar temperature profiles for all four depths (Figure 5). The soil water content at all depths was much lower in the sand than in the clay, reducing the penetration depth of freezing [6]. Furthermore, at 30 and 40 cm depth in the sand, there was little water left to freeze (30 cm: 0.08 $m^3 \cdot m^{-3}$; 40 cm: 0.06 $m^3 \cdot m^{-3}$).

When the combined rain and snowmelt event occurred in 2014 (Table 2), both soils had just started to thaw. During the event, similar soil water contents as measured before freezing (~0.25 $m^3 \cdot m^{-3}$) were reached in the clay. In the sand, soil water content at 5 cm depth initially rose rapidly above (~0.18 $m^3 \cdot m^{-3}$) pre-freezing values (~0.10 $m^3 \cdot m^{-3}$), but decreased to pre-freezing values during the event, while at the other three depths studied, the soil water content continued to increase during the whole event. At all four soil depths in both soils, the soil temperature rose significantly to above 0 °C, reaching the highest temperature (3.6 °C) at 5 cm.

The change in liquid soil water content in winter 2015 (Figure 4) was characterized by low values at 5 cm in both soils (minimum of 0.07 $m^3 \cdot m^{-3}$) due to early freezing in the beginning of December. This was followed by a decrease in liquid soil water content at 20, 30 and 40 cm in the clay on 17 December, reaching a minimum of 0.10 $m^3 \cdot m^{-3}$ at 20 and 30 cm and 0.14 $m^3 \cdot m^{-3}$ at 40 cm. A sudden increase in liquid soil water content occurred on 7 March at all depths in the clay and at 5 cm in the sand, when the air (Figure 2) and soil temperature (Figure 5) rose significantly to above 0 °C. In winter 2015, the rain event (Table 2) was preceded by freezing temperatures at 5–30 cm soil depth and low liquid soil water content at all soil depths in both soils (Figures 5 and 6). During the event, the liquid soil water content rose rapidly at 30 and 40 cm depth in the clay, reaching its highest value (0.42 $m^3 \cdot m^{-3}$) at 40 cm depth. At 5- and 20 cm depth, the change in liquid soil water content was less pronounced. Soil temperature rose in the upper three depths in both soils to about 0 °C, while at 40 cm depth, the soil temperature stayed above 0 °C at all times in both soils.

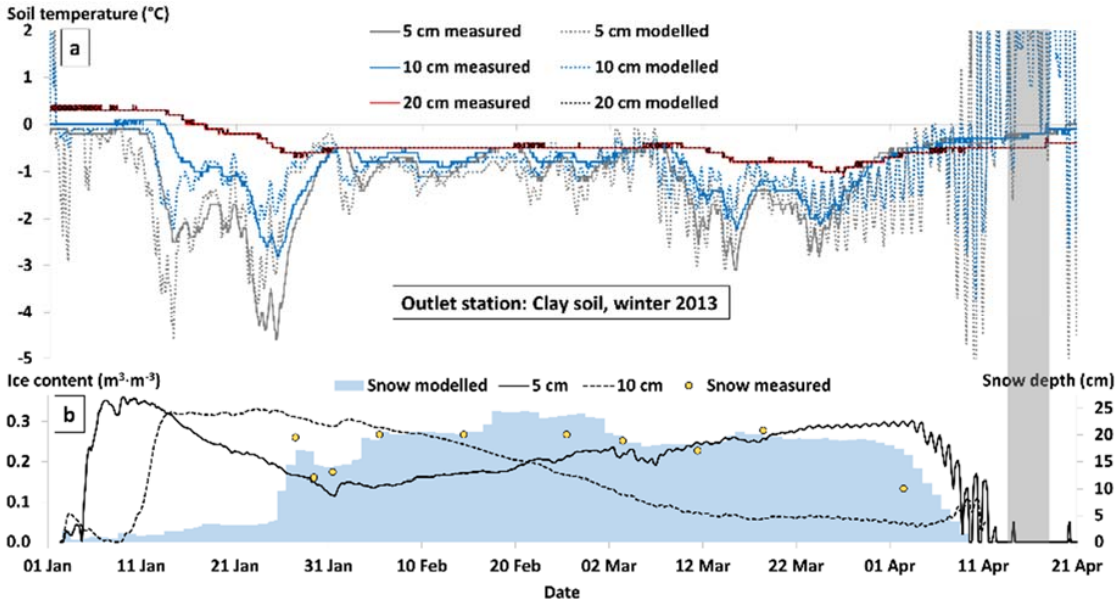


**Figure 6.** Diagram of (**a**) modelled and measured soil temperature at three depths (5, 10 and 20 cm) in the clay soil (at outlet station) during winter 2013; diagram of (**b**) measured and modelled snow depths at the outlet station and modelled ice content at the three depths in the clay soil (was zero at 20 cm). The duration of the rain event of interest is marked with a grey band.

### *3.4. SHAW Modelling*

The simulated snow depth, soil temperature and ice content values for the clay during winter 2013 are presented in Figure 6, for the clay and sand during winter 2014 in Figures 7 and 8 and for winter 2015 in Figures 9 and 10. As mentioned, due to missing measurements for the sand during winter 2013, the sand was not modelled for that year.

As can be seen from Figure 6, the SHAW model simulated the changes in the snow pack very accurately for 2013. To fit the simulated snow depth to the measured values, the $z_m$ parameter was set to 0.15 cm. The simulated soil temperature at 5 and 10 cm showed some fluctuations around the measured temperature, which increased after the snowpack disappeared in the end of March, when the air temperature fluctuated between −7 and 8 °C on a daily basis (Figure 2). However, it should be noted that the soil temperature was measured below a thick grass layer at the outlet station, and this grass layer probably acted as insulation [40], buffering the soil from the fluctuating air temperature. The model results show soil temperatures for bare ground, for comparison with the other winters. Due to the satisfactory simulation of snow depth and soil temperature, it was assumed that SHAW also performed well in simulating ice content in the soil profile. Simulated ice content was

high (0.35 $m^3 \cdot m^{-3}$) at 5 and 10 cm depth and zero at 20 cm depth, indicating that almost all of the water at these depths was frozen. The ice at these depths was apparently formed during the low soil temperatures in January, before the snow pack was established. SHAW was able to simulate the rise in soil temperature after the snow pack reached a depth of about 20 cm in February and predicted a decrease in ice content to zero at all depths by 12 April. The SHAW model was also able to simulate the observed decrease in soil temperature in the middle of April.

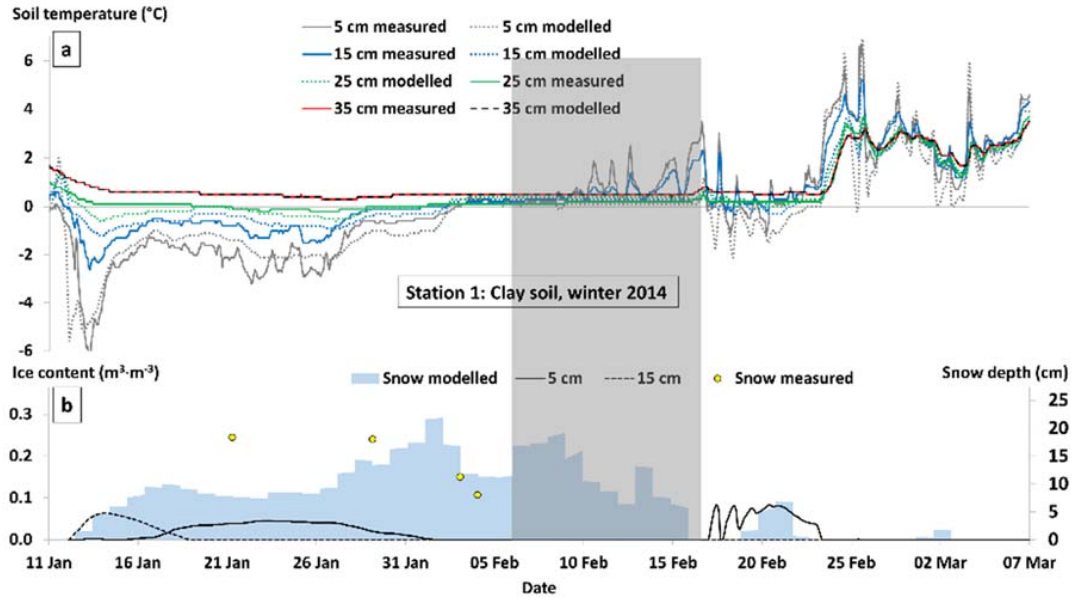


**Figure 7.** Diagram of (**a**) modelled and measured soil temperature at four depths (5, 10 and 20 cm) in the clay soil (at Station 1) during winter 2014; diagram of (**b**) measured and modelled snow depths at Station 1 and modelled ice content at four depths in the clay soil (was zero at 25 and 35 cm). The duration of the rain event of interest is marked with a grey band.

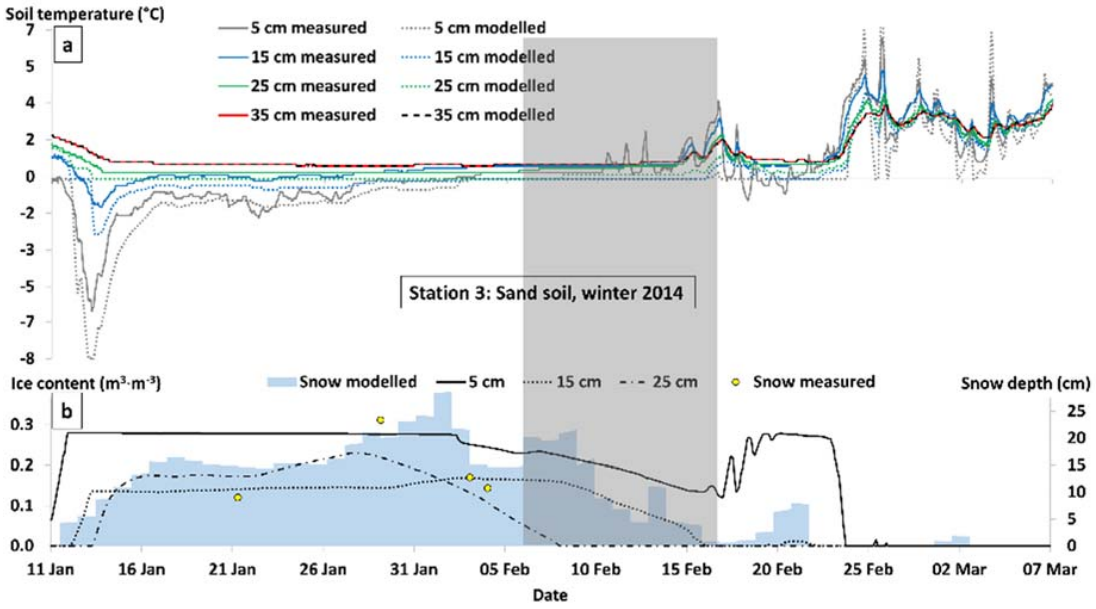


**Figure 8.** Diagram of (**a**) modelled and measured soil temperature at four depths (5, 15, 25 and 35 cm) in the sand soil (at Station 3) during winter 2014; diagram of (**b**) measured and modelled snow depths at Station 3 and modelled ice content at four depths in the sand soil (was zero at 35 cm). The duration of the rain event of interest is marked with a grey band.

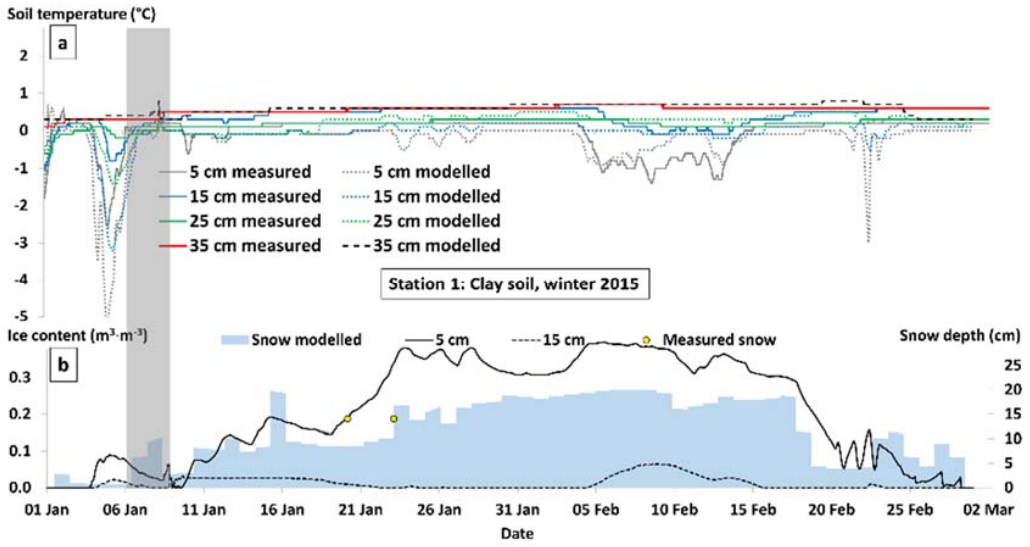


**Figure 9.** Diagram of (**a**) modelled and measured soil temperature at four depths (5, 15, 25 and 35 cm) in the clay soil (at Station 1) during winter 2015; diagram of (**b**) measured and modelled snow depths at Station 1 and modelled ice content at four depths in the clay soil (was zero at 25 and 35 cm). The duration of the rain event of interest is marked with a grey band.

Because only four snow depth measurements were possible in 2014, it was difficult to compare the simulated and measured snow depth values. However, it can be seen that SHAW underpredicted the snow depth above the clay soil during January and overpredicted it above the sand soil (Figures 7 and 8). The $z_m$ parameter was adjusted to 0.5 cm for the clay and 1.5 cm for the sand.

The simulated soil temperature in the clay soil (Figure 7) followed the measured temperature rather closely during the freezing period in January, but during the start of the snowmelt in the middle of February, the measured temperature showed a higher fluctuation than the simulated temperature. For the sand, SHAW simulated slightly lower temperature (−8 °C at 5 cm) than the measured values (−6 °C at 5 cm), but in general, the simulated temperature followed the trend in the measured data quite well (Figure 8). SHAW predicted low ice content for the clay at 5 and 15 cm (max. 0.06 $m^3 \cdot m^{-3}$ at 15 cm) and no ice at lower depths, while for the sand, it predicted an ice content of 0.28 $m^3 \cdot m^{-3}$ at 5 cm and 0.22 $m^3 \cdot m^{-3}$ at 25 cm depth. At 5 and 15 cm, the model predicted that all the available water was frozen, which can be seen as the constant ice contents between 12 January and 2 February. Moreover, the period with frozen water in the sand profile was considerably longer (11 January–23 February at 5 cm) than that in the clay (12 January–1 February at 5 cm).

Except for a slight underprediction of the snow depth for the period when the first two snow measurements were taken in 2015, SHAW simulated the snow depth well for winter 2015 (Figure 10). To obtain this fit, $z_m$ was set to 0.05 cm for the clay and 0.08 cm for the sand. In addition, $T_{max}$ had to be set to 3.8 °C to fit the modelled snow thicknesses to the measured, which resulted in the simulation of a thin snow cover, which did not occur in the field, during the rain event of interest in 2015. This adjustment of $T_{max}$ was in accordance with [32], who used a comparable snow model for the study area and had to make a similar adjustment to this parameter.

The simulated soil temperature showed similar low fluctuations as the measured (Figures 9 and 10), and the first negative peak was also simulated, with a good fit in the sand and slightly lower temperature in the clay (−5.8 °C simulated compared with −3 °C measured at 5 cm).

For both the clay and the sand, SHAW predicted high ice content at 5 cm depth, mainly during the period when the snow pack was between 10 and 20 cm thick (Figures 9 and 10). The predicted values were 0.39 $m^3 \cdot m^{-3}$ in the clay and 0.45 $m^3 \cdot m^{-3}$ in the sand. For both soils, SHAW simulated an increase in ice content at 5 cm with growing snow thickness and a decrease in ice content with decreasing snow thickness.

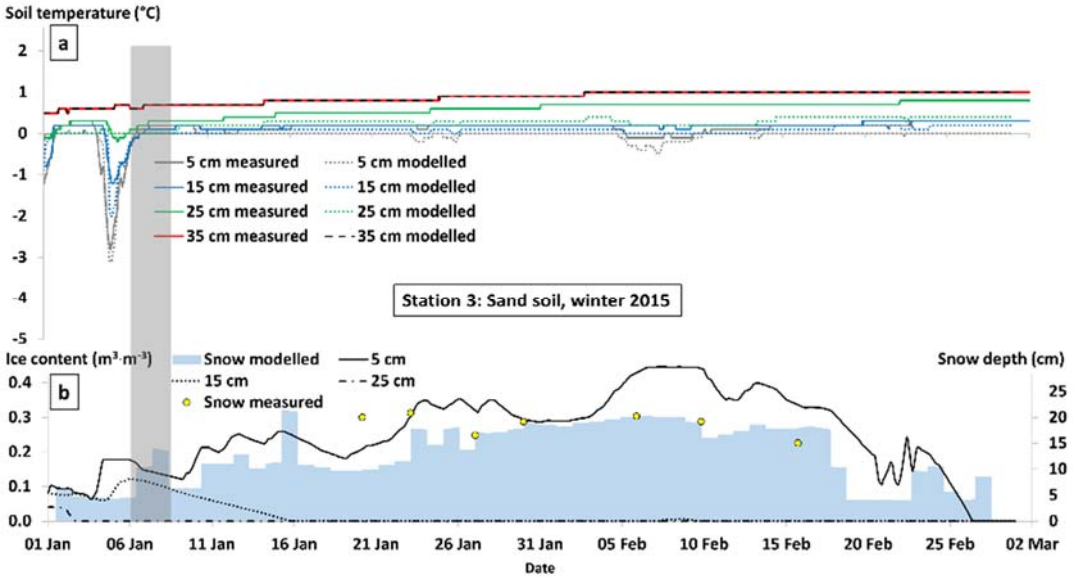


**Figure 10.** Diagram of (**a**) modelled and measured soil temperature at four depths (5, 15, 25 and 35 cm) in the sand soil (at Station 3) during winter 2015; diagram of (**b**) measured and modelled snow depths at Station 3 and modelled ice content at four depths in the sand soil (was zero at 35 cm). The duration of the rain event of interest is marked with a grey band.

### *3.5. Erosion Mapping*

During winter 2013, no erosion was observed anywhere in the catchment. The combined snowmelt and rain event in 2014 formed several small rills with a maximum width of 20 cm and 5–10 cm deep on two slopes in the catchment (Figure 11). The observed rills were formed mainly in the tracks created by the cultivator.

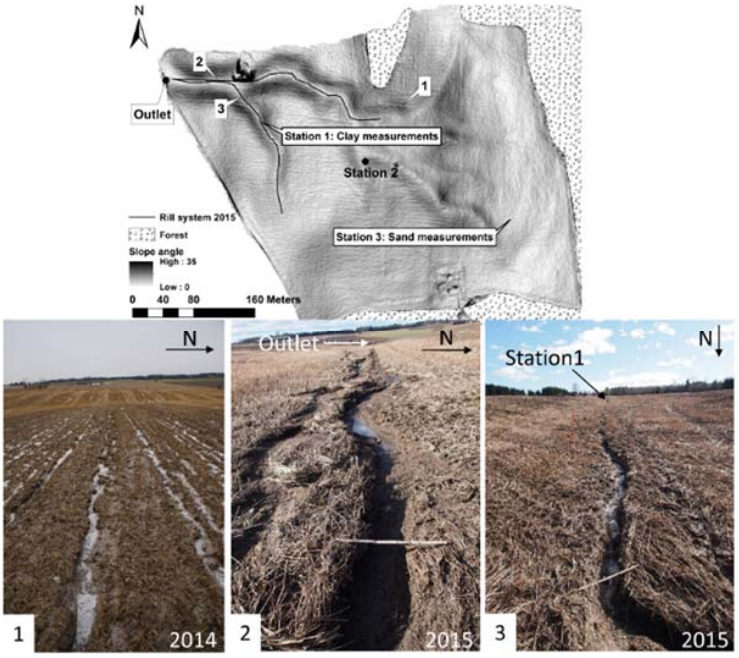


**Figure 11.** Slope angle map showing; the extent of the rill system, which formed during winter 2015 and the location where images 1–3 were taken. Image 1 shows rills which formed during the combined snowmelt and rain event in 2014 and images 2,3 show rills that formed during winter 2015.

In winter 2015, a continuous rill system (total length 493 m) was formed in depressions, where surface runoff was concentrated, during the main rain event. The rills varied in width and depth (Figure 11, Image 2,3), with measured maximum width of 40 cm and a depth of 20 cm. Several sedimentation areas were observed where the surface runoff was slowed down, due to reduced slope angle and increased flow width, indicating that not all of the eroded soil reached the outlet. At the other slope where rills were observed in 2014 (Figure 11, Image 1), the rills were connected to the extensive rill system in 2015.

## 4. Discussion

The winters of 2013, 2014 and 2015 differed significantly from each other in terms of the number of freezing periods, the length of period with a continuous snow cover and the number of rain events (Figure 2). The soils stayed frozen throughout the whole time with a continuous snow cover in the three winter periods, confirming the finding by Zhao et al. [15] that a thin (<25 cm) snow pack can increase soil freezing, e.g., due to an increase in ground albedo.

The amount of water that can infiltrate depends on the water permeability of the soil and the speed of surface runoff. In frozen soil, the water permeability depends on pre-freezing conditions [41], i.e., what the soil water content was before freezing started. In saturated soils the macropores are filled with water, which when frozen, clogs the pores. In the sand studied here, the initial soil water content was similar in 2013, 2014 and 2015, at between 0.10 and 0.25 $m^3 \cdot m^{-3}$, which is far below the measured saturation of 0.40–0.43 $m^3 \cdot m^{-3}$. Therefore, it can be assumed that the sand areas in the catchment contributed little to surface runoff during these three winters. This could explain why no erosion occurred in the depression on the sand soil in the catchment (Figure 1).

In the clay, however, the conditions differed between the years. In clays, water transport and infiltration capacity are highly dependent on macropores, particularly in the levelled clays found in the study area [42]. When freezing started in 2014, the clay had a soil water content of 0.25–0.30 $m^3 \cdot m^{-3}$, which according to the soil hydraulic characteristic curve for the clay represents a matric potential of 32 kPa (5 cm depth) to 315 kPa (20 cm depth), at which macropores are filled with air [43]. Furthermore, the rain event of interest in 2014 was less intensive than that in 2013 (Table 2), and the thawed soil allowed more water to infiltrate, resulting in a smaller amount of water reaching the outlet (Table 3). The SHAW results suggested that the clay was completely thawed by the time the rain event occurred (Figure 7).

However, despite a smaller discharge coefficient compared with 2013, the 2014 event caused erosion (Figure 11), in the tracks created by the cultivator.

Similarly to 2013, in winter 2015 the soil water content was 0.40–0.45 $m^3 \cdot m^{-3}$ at all soil depths in the clay when freezing started in November 2014, resulting in macropores filled with ice. Both events had a high discharge coefficient, of ~25% (50% when forest area was excluded) in 2013 and 32% (63%) during the first event in 2015 (Table 3). This, together with the low liquid soil moisture values, suggests that infiltration was restricted due to frozen soil during both events. Therefore, the fact that erosion did not occur in 2013, but did occur in 2015, cannot be explained by the infiltration capacity of the soil during the events. Moreover, the stability of the soils cannot explain the differences between 2013 and 2015, as confirmed by shear strength measurements carried out on the clay immediately before the event in 2013, which revealed low shear strength of 5–10 kPa at the soil surface (vane shear test, Eijkelkamp, The Netherlands).

Another process that could explain the differences between 2013 and 2015 is the speed of surface runoff, which determines the erosivity of surface runoff [44]. In 2013, the whole catchment was covered with stubble, but in 2015, only the depressions had intact stubble, while secondary tillage with a cultivator reduced the amount of plant residues on slopes. This tillage created a loose and smoother surface, probably causing higher speed of surface runoff, in freezing conditions in particular, as previously shown by Ban et al. [4]. This assumption was supported by the occurrence of soil erosion in the form of rills on the tilled slopes in 2014 (Figure 11). These findings were also in agreement with

Edwards and Burney [3], who concluded that only a plant cover can significantly reduce soil losses by rain and overland flow on frozen ground, e.g., through reduced runoff speeds and increased soil stability by roots. Our finding that the selected rain events on saturated and frozen soil produced a large amount of surface discharge confirmed the prediction by Stähli et al. [9] and Nyberg et al. [10] that high water saturation and early frost penetration, combined with heavy rain on still frozen soil, cause a marked increase in the amount of runoff.

Contrary to observation made by other studies (e.g., [21–23]), in all three winters studied, snowmelt played no significant role in terms of soil erosion. During snowmelt in 2014, the snow layer acted as a buffer for incoming rain. The rain infiltrated into the snow pack and surface runoff was delayed by the snow, reducing the erosive forces of the rain event. In 2013, no erosion occurred, and in 2015, the major soil erosion features had occurred before the first snow fell (Figure 2).

The performance of the SHAW model was satisfactory for all three winter periods. The change in soil temperature and snow pack was well reproduced, and the simulated ice content was in agreement with the measured liquid soil water content. In general, SHAW predicted ice in the soil for the periods when the FDR probes measured low liquid soil water contents. With the adjustment of two snow-related parameters in the model, it was possible to obtain reasonable results for the three different winter periods. Adjustment of $T_{max}$ for winters when snow falls at temperatures above 0 °C, as was the case in 2015, allows the model to partition incoming precipitation into snow and rain based on field observations, rather than using linear interpolation. The performance of SHAW in this study proved that it can be a valuable tool for investigating and predicting: (1) water content at freezing; (2) whether soil is frozen or unfrozen at a particular moment; and (3) the state of the snow cover. These are three important factors that control the amount of runoff during winter and are indispensable for predicting when soil erosion can be expected.

## 5. Conclusions and Implications

Field observations carried out during three winters in a catchment in southern Norway showed how soil hydraulic properties changed due to freezing-thawing, affecting surface runoff caused by snowmelt and rain, and how these processes are linked to soil erosion. The largest amount of soil erosion was caused by a small rain event on frozen ground, before the snow cover was established, while snowmelt played no significant role in terms of soil erosion. Four factors that determine the extent of runoff and erosion were of particular importance: (1) soil water content at freezing; (2) whether soil was frozen or unfrozen at a particular moment; (3) the state of the snow cover; and (4) tillage operations prior to winter. The simulation results showed that the SHAW model, with its accurate snow pack routine, is a useful tool that can help to investigate and identify non-tillage factors (e.g., 1, 2 and 3) influencing erosion.

**Acknowledgments:** This research was funded by the Catchy project of NIBIO, Norwegian Institute of Bioeconomy Research.

**Author Contributions:** T.S. conducted this research as part of his Ph.D. and conceived and designed this study, acquired the data, performed the modelling, analyzed and interpreted the data and wrote the paper. R.H., J.S. and C.R. supervised the work and helped with improving the manuscript.

**Conflicts of Interest:** The authors declare no conflict of interest.

## References

1. Ollesch, G.; Sukhanovski, Y.; Kistner, I.; Rode, M.; Meissner, R. Characterization and modelling of the spatial heterogeneity of snowmelt erosion. *Earth Surf. Process. Landf.* **2005**, *30*, 197–211. [CrossRef]
2. Iwata, Y.; Nemoto, M.; Hasegawa, S.; Yanai, Y.; Kuwao, K.; Hirota, T. Influence of rain, air temperature, and snow cover on subsequent spring-snowmelt infiltration into thin frozen soil layer in northern Japan. *J. Hydrol.* **2011**, *401*, 165–176. [CrossRef]
3. Edwards, L.M.; Burney, J.R. Soil erosion losses under freeze/thaw and winter ground cover using a laboratory rainfall simulator. *Can. Agric. Eng.* **1987**, *29*, 109–115.

4. Ban, Y.; Lei, T.; Liu, Z.; Chen, C. Comparison of rill flow velocity over frozen and thawed slopes with electrolyte tracer method. *J. Hydrol.* **2016**, *534*, 630–637. [CrossRef]
5. Watanabe, K.; Kito, T.; Dun, S.; Wu, J.Q.; Greer, R.C.; Flury, M. Water Infiltration into a Frozen Soil with Simultaneous Melting of the Frozen Layer. *Vadose Zone J.* **2013**, *12*. [CrossRef]
6. Yami, E.R.; Khalili, A.; Rahimi, H.; Etemad, A. Investigation of moisture on soil temperature regimes and frost depths in a laboratory model. *Int. J. Agric. Sci.* **2012**, *2*, 717–732.
7. Al-Houri, Z.M.; Barber, M.E.; Yonge, D.R.; Ullman, J.L.; Beutel, M.W. Impact of frozen soils on the performance of infiltration treatment facilities. *Cold Reg. Sci. Technol.* **2009**, *59*, 51–57. [CrossRef]
8. Willis, W.O.; Carlson, C.W.; Alessi, J.; Haas, H.J. Depth of freezing and spring run-off as related to fall soil-moisture level. *Can. J. Soil Sci.* **1961**, *41*, 115–123. [CrossRef]
9. Stähli, M.; Nyberg, L.; Mellander, P.; Jansson, P.; Bishop, K.H. Soil forst effects on soil water and runoff dynamics along a boreal transect: 2. Simulations. *Hydrol. Process.* **2001**, *15*, 927–941. [CrossRef]
10. Nyberg, L.; Stähli, M.; Mellander, P.; Bishop, K.H. Soil frost effect on soil water and runoff dynamics along a boreal forest transect: 1. Field investigations. *Hydrol. Process.* **2001**, *15*, 909–926. [CrossRef]
11. Lindström, G.; Löfvenius, M.O. *Tjäle Och Avrinning i Svartberget—Studier Med HBV-Modellen*; SMHI hydrologi Nr 84; SMHI: Norrköping, Sweden, 2000.
12. Iwata, Y.; Hayashi, M.; Suzuki, S.; Hirota, T.; Hasegawa, S. Effects of snow cover on soil freezing, water movement, and snowmelt infiltration: A paired plot experiment. *Water Resour. Res.* **2010**, *46*, 1–11. [CrossRef]
13. Zhao, Y.; Nishimura, T.; Hill, R.; Miyazaki, T. Determining Hydraulic Conductivity for Air-Filled Porosity in an Unsaturated Frozen Soil by the Multistep Outflow Method. *Vadose Zone J.* **2013**, *12*. [CrossRef]
14. Sutinen, R.; Hänninen, P.; Venäläinen, A. Effect of mild winter events on soil water content beneth snowpack. *Cold Reg. Sci. Technol.* **2008**, *51*, 56–67. [CrossRef]
15. Zhao, Y.; Huang, M.B.; Horton, R.; Liu, F.; Peth, S.; Horn, R. Influence of winter grazing on water and heat flow in seasonal frozen soil of Inner Mongolia. *Vadose Zone J.* **2013**, *12*. [CrossRef]
16. Parkin, G.; von Bertoldi, A.P.; McCoy, A.J. Effect of tillage on Soil Water Content and Temperature under Freeze-Thaw Conditions. *Vadose Zone J.* **2013**, *12*. [CrossRef]
17. He, H.; Dyck, M.F.; Si, B.C.; Zhang, T.; Lv, J.; Wang, J. Soil freezing—Thawing characteristics and snowmelt infiltration in Cryalfs of Alberta, Canada. *Geodermal. Reg.* **2015**, *5*, 198–208. [CrossRef]
18. Kormos, P.R.; Marks, D.; Williams, C.J.; Marshall, H.P.; Aishlin, P.; Chandler, D.G.; McNamara, J.P. Soil, snow, weather, and sub-surface storage data from a mountain catchment in the rain-snow transition zone. *Earth Syst. Sci. Data* **2014**, *6*, 165–173. [CrossRef]
19. Williams, C.J.; Mcnamara, J.P.; Chandler, D.G. Controls on the temporal and spatial variability of soil moisture in a mountainous landscape: The signature of snow and complex terrain. *Hydrol. Earth Syst. Sci.* **2009**, *13*, 1325–1336. [CrossRef]
20. Shanley, J.B.; Chalmers, A. The effect of frozen soil on snowmelt runoff at Sleepers River, Vermont. *Hydrol. Process.* **1999**, *13*, 1843–1857. [CrossRef]
21. Lundekvam, H.; Skøien, S. Soil erosion in Norway. An overview of measurements from soil loss plots. *Soil Use Manag.* **1998**, *14*, 84–89. [CrossRef]
22. Deelstra, J.; Kværnø, S.H.; Granlund, K.; Sileika, A.S.; Gaigalis, K.; Kyllmar, K.; Vagstad, N. Runoff and nutrient losses during winter periods in cold climates—Requirements to nutrient simulation models. *J. Environ. Monit.* **2009**, *11*, 602–609. [CrossRef] [PubMed]
23. Øygarden, L. Rill and gully development during an extreme winter runoff event in Norway. *Catena* **2003**, *50*, 217–242. [CrossRef]
24. Grønsten, H.A.; Lundekvam, H. Prediction of surface runoff and soil loss in southeastern Norway using the WEPP Hillslope model. *Soil Tillage Res.* **2006**, *85*, 186–199. [CrossRef]
25. Flerchinger, G.N.; Xiao, W.; Sauer, T.J.; Yu, Q. Simulation of within-canopy radiation exchange. *NJAS Wagening. J. Life Sci.* **2009**, *57*, 5–15. [CrossRef]
26. Hansen, N.C.; Gupta, S.C.; Moncrief, J.F. Snowmelt runoff, sediment, and phosphorous losses under three different tillage systems. *Soil Tillage Res.* **2000**, *57*, 93–100. [CrossRef]
27. Govers, G. Rill erosion on arable land in central Belgium: Rates, controls and predictability. *Catena* **1991**, *18*, 133–155. [CrossRef]

28. Boardman, J.; Shepheard, M.L.; Walker, E.; Foster, I.D.L. Soil erosion risk-assessment for on- and off-farm impacts: A test case using the Midhurst area, West Sussex, UK. *J. Environ. Manag.* **2009**, *90*, 2578–2588. [CrossRef] [PubMed]
29. Weigert, A.; Schmidt, J. Water transport under winter conditions. *Catena* **2005**, *64*, 193–208. [CrossRef]
30. Yakutina, O.P.; Nechaeva, T.V.; Smirnova, N.V. Consequences of snowmelt erosion: Soil fertility, productivity and quality of wheat on Greyzemic Phaeozem in the south of West Siberia. *Agric. Ecosyst. Environ.* **2015**, *200*, 88–93. [CrossRef]
31. Su, J.J.; van Bochove, E.; Thériault, G.; Novotma, B.; Khaldoune, J.; Denault, J.T.; Zhou, J.; Nolin, M.C.; Hu, C.X.; Bernier, M.; et al. Effects of snowmelt on phosphorus and sediment losses from agricultural watersheds in Eastern Canada. *Agric. Water Manag.* **2011**, *98*, 867–876. [CrossRef]
32. Kramer, G.J.; Stolte, J. *Cold-Season Hydrologic Modeling in the Skuterud Catchment. An Energy Balance Snowmelt Model Coupled with a GIS-Based Hydrology Model*; Bioforsk Report 4(126); Bioforsk: Ås, Norway, 2009; Volume 46.
33. Thue-Hansen, V.; Grimenes, A.A. *Meteorologiske Data for Ås*; Norges Miljø og Biovitenskaplige Universitet: Ås, Norway, 2013–2014.
34. Kværnø, S.H.; Øygarden, L. The influence of freeze-thaw cycles and soil moisture on aggreagte stability of three soils in Norway. *Catena* **2006**, *67*, 175–182. [CrossRef]
35. Starkloff, T.; Stolte, J.; Hessel, R.; Ritsema, C. Understanding snowpack development at catchment scale, using comprehensive field observations and spatially distributed snow modelling. *Hydrol. Res.* **2017**, in press.
36. Flerchinger, G.N.; Saxton, K.E. Simultaneous heat and water model of a freezing snow-residue-soil system. I. Theory and development. *Trans. Am. Soc. Agric. Eng.* **1989**, *32*, 565–571. [CrossRef]
37. Li, R.; Shi, H.; Flerchinger, G.N.; Akae, T.; Wang, C. Simulation of freezing and thawing soils in Inner Mongolia Hetao Irrigation District China. *Geoderma* **2012**, *173*, 28–33. [CrossRef]
38. Flerchinger, G.N. *The Simultaneous Heat and Water (SHAW) Model: Technical Documentation*; Technical Report NWRC 2000-09; Northwest Watershed Research Center, USDA Agricultural Research Service: Boise, ID, USA, 2000.
39. Black, C.A.; Evans, D.D.; White, J.L.; Ensminger, L.E.; Clark, F.E. *Methods of Soil Analysis Physical and Mineralogical Properties, Including Statistics of Measurement and Sampling*; American Society of Agronomy: Madison, WI, USA, 1965; Part 1, Volume 9, pp. 1–770.
40. Flerchinger, G.N.; Sauer, T.J.; Aiken, R.A. Effects of crop residue cover and architecture on heat and water transfer at the soil surface. *Geoderma* **2003**, *116*, 217–233. [CrossRef]
41. McCauley, C.A.; White, D.M.; Lilly, M.R.; Nyman, D.M. A comparison of hydraulic conductivities, permeabilities and infiltration rates in frozen and unfrozen soils. *Cold Reg. Sci. Technol.* **2002**, *34*, 117–125. [CrossRef]
42. Øygarden, L.; Kværner, J.; Jenssen, P.D. Soil erosion via preferential flow to drainage systems in clay soils. *Geoderma* **1997**, *76*, 65–86. [CrossRef]
43. Lundberg, A.; Ala-Aho, P.; Eklo, O.; Klöve, B.; Kværner, J.; Stumpp, C. Snow and frost: Implications for spatiotemporal infiltration patterns—A review. *Hydrol. Process.* **2015**, *30*, 1230–1250. [CrossRef]
44. Boardman, J.; Poesen, J. *Soil Erosion in Europe*; John Wiley & Sons Inc.: Hoboken, NJ, USA, 2006; p. 855.